Macromelecules

pubs.acs.org/Macromolecules Article

Cooperative Self-Assembly of Lipid–Polymer Hybrids Stabilizing Highly Ordered Bicontinuous Cubic Phases in Air

Minjee Kang, Yoo Kyung Go, Marilyn Porras-Gomez, Tzortzis Koulaxizis, Dylan Steer, Antonia Statt,* and Cecilia Leal*

Cite This: *Macromolecules* 2023, 56, 5774–5783 Read Online

ACCESS | Metrics & More | Article Recommendations | Supporting Information

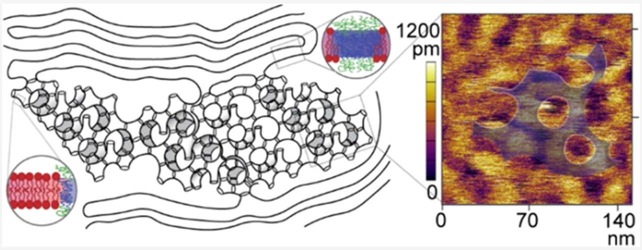

ABSTRACT: The co-assembly of lipids and block copolymers is a new strategy to enable materials with nanostructure complexity as well as responsive transport and mechanical behavior. In water, lipids adopt a variety of structures including bicontinuous cubic phases that are highly desirable for numerous biotechnological applications and separation membranes. Block polymers assemble into analogous mesophases but do not always require aqueous media. Using grazing incidence small-angle X-ray scattering (GISAXS) and atomic force microscopy (AFM), we show that monoolein (MO), 1,2-dioleoyl-3-trimethylammonium-propane (DOTAP), and poly(butadiene-*b*-ethylene oxide) (PBD-*b*-PEO) self-organize into highly ordered bicontinuous cubic phases without the need of an aqueous environment. Ternary MO/DOTAP/PBD-*b*-PEO systems exhibit hybrid bilayer networks separating periodic arrays of nonpenetrating channels retaining water from air humidity. We attribute this behavior to positively charged lipids that in cooperation with block copolymers can pin ambient hydration, demonstrated by coarse-grained simulations. Our study broadens the understanding of the structural diversity of lipid–polymer hybrid materials, opening the potential of designing new biocompatible humidity-responsive nanomaterials.

■ INTRODUCTION

Co-self-assembly of amphiphilic lipids and block copolymers (BCP) has fascinated a number of soft matter scientists over the past decade as a means to combine the advantages of both molecular systems in a single hybrid structure.[1−11] Phospholipids are abundant membrane lipids in nature, providing excellent biocompatibility and ability to aggregate into various structures in aqueous environments. Compared with lipids, BCPs have chemical versatility to modulate functional groups but come with a drawback of lower biocompatibility and being less dynamic when transforming from one phase to another. Some block polymers are amphiphilic like lipids and assemble in water into a variety of mesophases, while others can stabilize nanostructures in air.[12] Lipid–BCP hybrid membranes have synergistic structural and functional properties otherwise not achievable with the assembly of single components. Previous studies reported advanced properties of the lipid–polymer co-assemblies, e.g., improved mechanical stability,[13−15] controllable solubility of encapsulated solutes in membranes,[16−20] synergistic permeability of cargo drugs,[20−22] and control of polymer crystallization and thermal properties.[2,23] Research on lipid–BCP hybrid membranes has been mainly conducted on lamellar systems in the form of vesicles dispersed in water,[24,25] monolayer suspended in water,[18] or bilayers on solid supports,[26−28] leaving a gap in our understanding of polymorphism of the lipid–BCP hybrid system. Nonetheless, lipid–BCP mixtures hold a huge potential in creating nonlamellar structures with increasingly complex structures and topologies given that each amphiphile has the ability to self-assemble into various nanostructures. Indeed, recent studies on lipid–BCP hybrid membranes revealed more complex structures, e.g., patched surfaces[19,23,25] and compartmentalized domains stacked in registry across multilayers.[2,21,29]

In this paper, we investigate the polymorphism of a lipid–BCP hybrid system composed of monoolein (MO), 1,2-dioleoyl-3-trimethylammonium-propane (DOTAP), and poly(butadiene-*b*-ethylene oxide) (PBD-*b*-PEO) by changing relative composition and relative humidity (RH). Using grazing incidence small-angle X-ray scattering (GISAXS) and atomic force microscopy (AFM), we constructed a partial ternary phase diagram displaying a rich variety of structures including one-dimensional (1D)-lamellar, two-dimensional (2D)-inverted hexagonal, and three-dimensional (3D)-bicontinuous cubic phases.

Received: February 10, 2023
Revised: May 31, 2023
Published: July 25, 2023

https://doi.org/10.1021/acs.macromol.3c00239

Inverse bicontinuous cubic phases (Q_{II}) are three-dimensional nanostructures where amphiphiles form a triple periodic bilayer dividing the space into two percolating but non-intersecting water channels. Due to their unique geometry, high surface area, and channel network, Q_{II} phases have gained attention in the field of drug delivery, protein crystallization, and crystallography, and are highly desirable as separation membranes.[30−33] One of the challenges in applications comes from the nature of the Q_{II} phases that require an aqueous environment to maintain their structure.[34,35] For example, membrane protein crystallization processes using lipid Q_{II} templates[31] can take a few days to months and it is challenging to maintain Q_{II} integrity when exposed to air. There have been important efforts to improve the stability of lipid Q_{II} phases in a low-humidity environment, making them ″less volatile″ by adding sugar, glycerol,[36] or salts[35] that replace water molecules in water channels. In this paper, we discovered that judicious control over the composition of MO/DOTAP/PBD-*b*-PEO hybrid systems results in unusually stable Q_{II} phases in air. Using coarse-grained molecular dynamics simulations, we show the role of PEO chains in retaining water as the channel is dehydrated and the effect of the positively charged DOTAP headgroups in providing an energetic benefit to surrounding Cl^- ions that can pin ambient hydration in cooperation with PEO chains. This work highlights the importance of studying polymorphism of lipid−polymer hybrid composites, providing insight into the cooperative self-assembly behavior of lipids and BCPs essential for functional hybrid materials design.

■ RESULTS AND DISCUSSION

Self-assembly building blocks used in this work are monoolein (MO), 1,2-dioleoyl-3-trimethylammonium-propane (DOTAP), and poly(butadiene-*b*-ethylene oxide) (PBD-*b*-PEO) whose chemical structures are shown in Figure 1A.

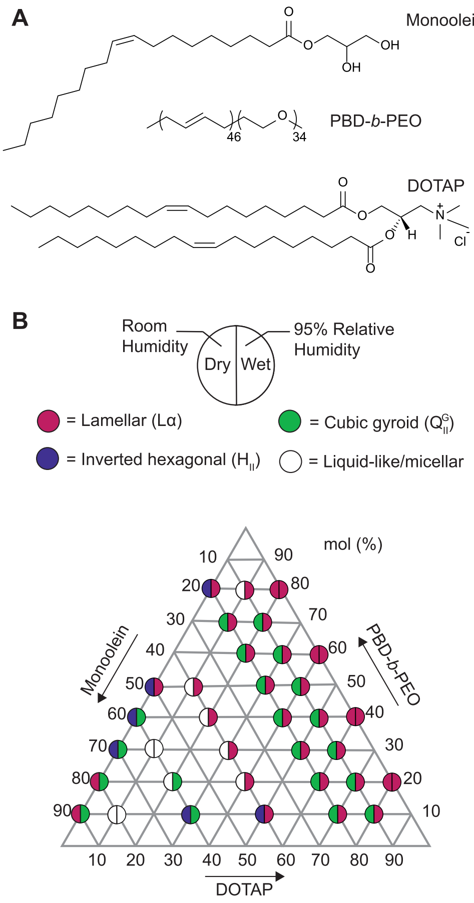

Figure 1. Rich phase behavior of lipid−polymer hybrid films on solid supports. (A) Chemical structures of monoolein (MO), 1,2-dioleoyl-3-trimethylammonium-propane (DOTAP), and poly(butadiene-*b*-ethylene oxide) (PBD-*b*-PEO). (B) Partial ternary phase diagram of lipid−polymer hybrid systems comprising MO, DOTAP, and PBD-*b*-PEO in the form of thin films at room temperature. Left semicircle indicates the phase measured in an open environment at ambient room humidity of 20−40% RH, and right semicircle indicates the phase measured in a closed environment at a high humidity (∼95% RH) using GISAXS. Red, blue, green, and white colors denote lamellar, inverted hexagonal, bicontinuous cubic gyroid, and micellar structures, respectively.

Monoolein (MO), or glyceryl monooleate, is a well-known lipid for forming various liquid crystalline self-assembled structures on exposure to excess water. At high water content, MO self-assembles into inverse bicontinuous cubic phases: the double gyroid phase (Q_{II}^{G}) up to 30 wt % water and the double diamond phase (Q_{II}^{D}) between 30 to 40 wt % water. At lower water content, dehydrated Q_{II} phases break down transforming into fluid lamellar (L_α) or inverse micellar structures (H_{II}). DOTAP is a univalent cationic lipid that in combination with MO is stable in various self-assembled structures.[37,38] In dry conditions (20−40% RH), MO/DOTAP systems showed either a 2D-inverted hexagonal phase (H_{II}) or a lamellar phase (L_α), whereas in wet conditions (>95% RH), MO/DOTAP showed a gyroid cubic phase (Q_{II}^{G}). Amphiphilic PBD-*b*-PEO, is often used to assemble synthetic bilayers for reconstituting membrane proteins because of its lyotropic phase behavior and good biocompatibility.[6,39] The hydrophobic PBD block has a low glass-transition temperature of about −10 °C. The hydrophilic PEO segment imparts good biocompatibility to the copolymer and is water soluble. We hypothesized that mixing of MO, DOTAP, and PBD-*b*-PEO would enable rich phase behavior that is highly dependent on water content. Consistent with our hypothesis, MO/DOTAP/PBD-*b*-PEO mixtures exhibit structural diversity in dry and wet conditions at room temperature. Figure 1B summarizes the phase behavior of mixtures in a partial ternary phase diagram studied using GISAXS. The left semicircle indicates the phase obtained in an open environment at ambient room humidity while the right semicircle indicates the phase obtained in a closed environment (∼95% RH).

Figure 2A shows GISAXS patterns of 3D-bicontinuous cubic (Q_{II}^{G}), 2D-inverted hexagonal (H_{II}), and 1D-lamellar structures (L_α) observed from different compositions of MO/DOTAP/PBD-*b*-PEO films. Diffraction patterns in Figure 2A indicate that domains in polycrystalline films are aligned with respect to the substrate in a way that minimizes the interfacial energy between substrate and domains. In the Q_{II}^{G} phase, (211) lattice planes are mainly oriented parallel to the substrate.[38] In the H_{II} phase, a honeycomb array of tubes is preferentially aligned parallel to the substrate as schematically depicted on top of Figure 2A. The L_α phase bilayer membranes are mostly stacked parallel to the substrate.

Surprisingly, we found that MO/DOTAP/PBD-*b*-PEO systems display gyroid cubic phases over a broad range of PBD-*b*-PEO content at ambient room humidity at fixed MO concentration (20 mol %). Figure 2B emphasizes the regime of dry cubic phases in lipid−polymer hybrid mixtures. Notably, at the same concentration of MO, MO/DOTAP binary mixtures

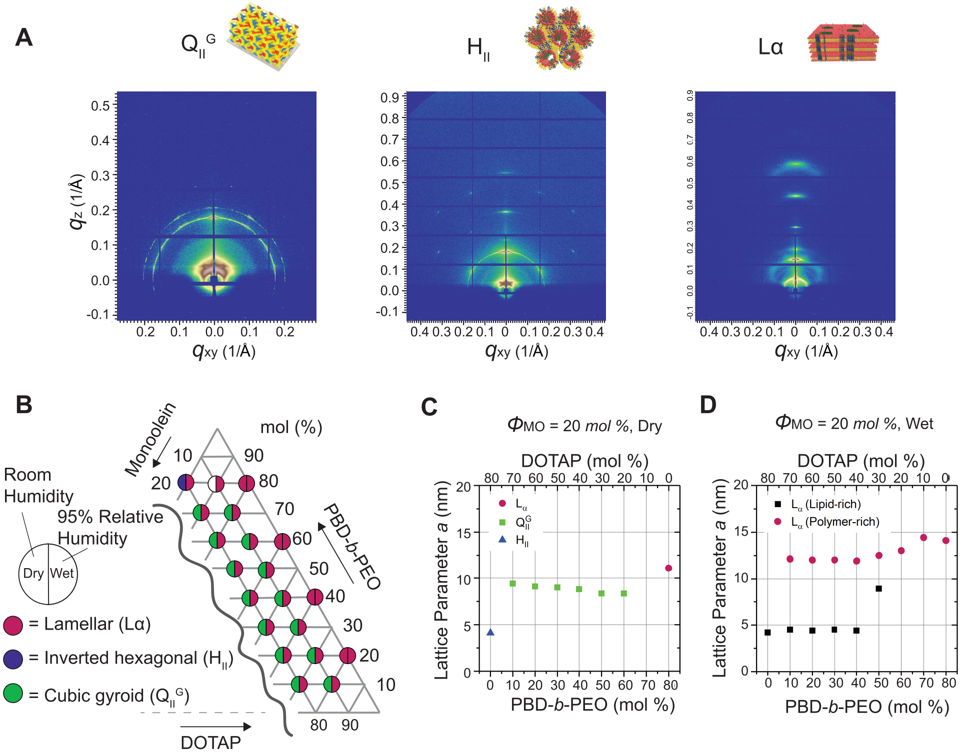

Figure 2. Gyroid cubic phases observed in dry MO/DOTAP/PBD-*b*-PEO films. (A) Representative GISAXS images of Q_{II}^G, H_{II}, and L_α phases formed from MO/DOTAP/PBD-*b*-PEO mixtures from left to right. Schematic illustrations of each phase are on the top of the images. (B) Partial ternary phase diagram of MO/DOTAP/PBD-*b*-PEO thin films. Left semicircle indicates the phase measured in an open environment at a typical ambient room humidity, and right semicircle indicates the phase measured in a closed environment at high humidity (~95% RH) using GISAXS. (C, D) Lattice parameter of MO/DOTAP/PBD-*b*-PEO films in (C) dry and (D) wet conditions. Red, blue, green, and white colors denote lamellar, inverted hexagonal, bicontinuous cubic gyroid, and micellar structures, respectively.

(20:80) do not form Q_{II}^G phases at any water content. The MO/DOTAP binary lipid mixtures form Q_{II}^G phases only when MO is a dominant component over DOTAP (90:10 to 60:40, molar percentage) and in excess water. Upon exposure to air, they readily transform into either H_{II} or L_α phases. This observation implies the involvement of PBD-*b*-PEO in forming Q_{II}^G phases at low humidity. To better understand the structures of MO/DOTAP/PBD-*b*-PEO hybrid phases, we calculated the lattice parameters from GISAXS $I(q)$ data as summarized in Figure 2C (dry) and Figure 2D (wet). At fixed MO concentration (20 mol %), the lattice parameter a (Q_{II}^G) is in the range of 9.4−8.35 nm, comparable to that of MO/DOTAP films[38] where a (Q_{II}^G) = 9.3 nm in dry conditions. The lattice parameter decreases in a dose-dependent manner as PBD-*b*-PEO content increases in Figure 2C.

PEO is a well-known water retention agent widely used in biomedical applications *e.g.* in contact lens solutions to prevent dehydration.[40] If PBD-*b*-PEO molecules are not colocalized with lipids at the molecular level but simply co-exist as a completely segregated component, they are likely to absorb water molecules from the MO/DOTAP lipid mixtures. This scenario is not consistent with the observed $L_\alpha \rightarrow Ia3d$ transformation in MO/DOTAP/PBD-*b*-PEO systems as the water content decreases while the MO−water system undergoes $Pn3m$ (Q_{II}^D) → $Ia3d$ (Q_{II}^G) → L_α upon dehydration.[41] Thus, a more plausible explanation of the appearance of the Q_{II}^G in dry conditions is that PBD-*b*-PEO cooperatively interacts with MO and DOTAP to facilitate packing of lipids and BCPs into inverse curvature membranes. The hydrophilicity of PEO may facilitate water retention in the nanochannels of the Q_{II}^G phase preventing water evaporation into the surrounding vapor. A similar principle has been applied to prevent the dehydration of cubic phases by Richardson et al.[36] They added glycerol to the MO lipid thin films replacing water with a water−glycerol mixture in the cubic phase water channels. They proposed inclusion of glycerol lowered the chemical potential of water molecules in the cubic phase water channels, thus lowering water vapor pressure and making the cubic phase less volatile.[36] The observed decrease in lattice parameter (Figure 2C) could be attributed to osmotic pressure exerted by hydrophilic PEO chains, more specifically PBD-*b*-PEO blocks not participating in the formation of a gyroid cubic phase as PBD-*b*-PEO content increases.

Excess water drives (Q_{II}^G) → L_α phase transformations in MO/DOTAP/PBD-*b*-PEO mixtures (Figure 2D). At high PBD-*b*-PEO content (60−80 mol %), a single L_α phase is present with lattice parameter a = 14.4 nm. At fixed MO = 20 mol % and DOTAP contents above 30 mol %, MO/DOTAP/PBD-*b*-PEO starts to form two distinct lamellar phases with different lattice parameters. In excess water conditions, the hydrophobic effect becomes more significant leading to significant PBD packing frustration into a continuously curved bilayer of a bicontinuous cubic phase. Even though the placement of PEO polymer chains into fully hydrated channels is entropically favorable due to the release of the hydrogen-bonded water molecules from PEO chains, this cannot compensate for the packing frustration of PBD blocks in continuously curved bilayers. This could explain the transformation of the Q_{II}^G phase into a phase-separated double lamellar MO/DOTAP/PBD-*b*-PEO system upon hydration.

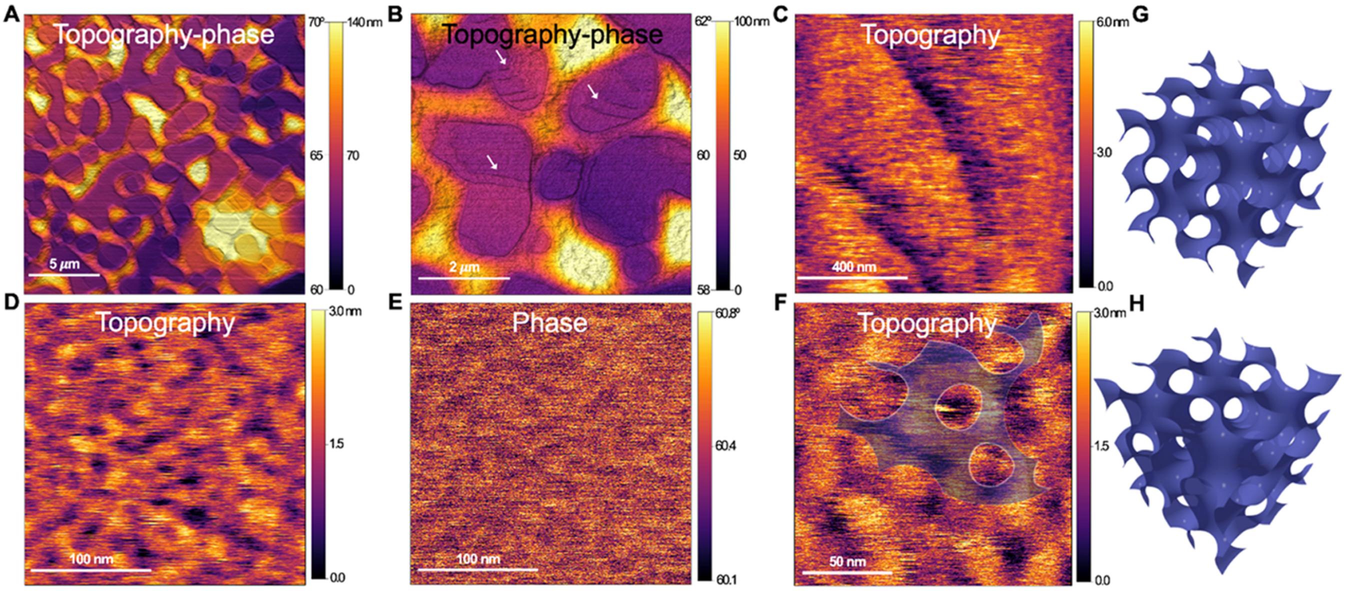

Figure 3. AFM mapping and visualization of gyroid structures of hybrid films in air. (A–F) AFM tapping mode topography and phase maps of various length scales of supported MO/DOTAP/PBD-*b*-PEO films in the gyroid phase at ambient room humidity. (A) Topography-phase 3D map, scan size 20 μm × 20 μm. (B) Topography-phase map, scan size of about 6 μm × 6 μm. (C) Topography map, scan size of 1 μm × 1 μm. (D) Topography map, scan size of about 200 nm × 200 nm. (E) Phase map, scan size of about 150 nm × 150 nm. An illustration of the surface unit cell lattice is overlaid. (F) Phase map corresponding to (E). (G–H) Rendered gyroid isosurfaces from two different perspectives.

One lamellar phase is lipid (MO/DOTAP)-rich, while another is a polymer (PBD-*b*-PEO)-rich phase (Figure 2D). The double lamellar systems are consistent with previous observations in DPPC/PBD-*b*-PEO binary mixtures where DPPC-rich and PBD-*b*-PEO-rich domains align in registry across multilayers.[1,2,21,23]

Another noteworthy aspect of the partial ternary phase diagram (Figure 2B) is that MO/PBD-*b*-PEO binary mixtures always form lamellar phases regardless of humidity and compositional changes. Without DOTAP, PBD-*b*-PEO fails to cooperate with MO to form a gyroid cubic phase. Only when DOTAP is added, MO/DOTAP/PBD-*b*-PEO mixtures exhibit cubic phases in air at low relative humidity. This highlights the role of DOTAP in "bridging" the interaction between MO and PBD-*b*-PEO. Grazing incidence wide-angle X-ray scattering (GIWAXS) was employed to prove the packing of MO, PBD-*b*-PEO, and DOTAP at the molecular level. Supporting Figure 1A shows GIWAXS one-dimensional $I(q)$ data obtained for neat lipid (MO/DOTAP) and neat polymer (PBD-*b*-PEO and homopolymer PEO) systems. The $I(q)$ data obtained for crystalline homopolymer PEO displays (110), (120), (121), (112), and (032) reflections arising from PEO crystalline domains. The $I(q)$ plot for PBD-*b*-PEO displays the diffraction peaks originating from PEO (120), (112), and (032) crystal planes indicating the existence of PEO microcrystallites, as well as a broad amorphous halo peak attributed to amorphous PBD blocks. GIWAXS results for MO/DOTAP films shows a broad Bragg ring arising from scattering between fluidic lipid tails in the L_α phase of MO/DOTAP assemblies mixed at the molecular level. Similarly, the $I(q)$ data acquired for MO/PBD-*b*-PEO hybrid mixtures demonstrates that sharp Bragg peaks originating from highly crystalline MO assemblies in an L_c phase[41] get much broader when PBD-*b*-PEO is added (Supporting Figure 1B). This result also illustrates MO and PBD-*b*-PEO mixing, most likely of MO hydrocarbon tails and the hydrophobic PBD block. The GIWAXS $I(q)$ plot for all three components shows broadening of the peak from carbon chain diffraction as the MO/DOTAP content increases (at fixed 6 mol % PBD-*b*-PEO), indicating that MO/DOTAP molecules fluidize hydrophobic membrane core (Supporting Figure 1C). It is noteworthy that GIWAXS data arising from PEO (hydrophilic) are consistent with the presence of semicrystalline domains in the MO/DOTAP/PBD-*b*-PEO hybrid films. Here, mixing of lipid sand polymers in a hybrid membrane occurs mainly among their hydrophobic moieties. Suggested molecular arrangements in MO/DOTAP/PBD-*b*-PEO hybrid films and the role of DOTAP to fluidize the hybrid membrane are illustrated in Supporting Figure 1D.

The phase diagram constructed using GISAXS (Figure 1B) demonstrates a cooperative self-assembly behavior in MO/DOTAP/PBD-*b*-PEO hybrid mixtures. However, GISAXS is an averaging technique that cannot provide information on the boundary region between adjacent domains, epitaxy, or domain size. In this regard, we performed AFM experiments to obtain topography and domain information on the structure of the supported amphiphile films. AFM imaging using ultrasharp tips on supported Q_{II}^{G} phases in air allowed the direct visualization of the bicontinuous cubic structure and film epitaxy at different length scales (Figure 3A–F).

We observe that the supported MO/DOTAP/PBD-*b*-PEO films in the gyroid phase exhibit poly-domains and sharp domain boundaries (Figure 3A–C) suggesting a system with multiscale molecular organization. Within each domain, there are terrace-like features that are consistent with multilayer structures (indicated by white arrows in Figure 3B). Increasing the magnification of AFM scans on these regions of interest revealed that the presence of interconnected domains (Figure 3D). This observation is consistent with the coexistence of bicontinuous cubic ((Q_{II}^{G}) and lamellar L_α phases) in the MO/DOTAP/PBD-*b*-PEO hybrid system as presented by GISAXS data (Figure 2A). The unit cell size of the Q_{II}^{G} phase can be estimated by AFM as $a = 9$ nm (Figure 3D,E) which is within

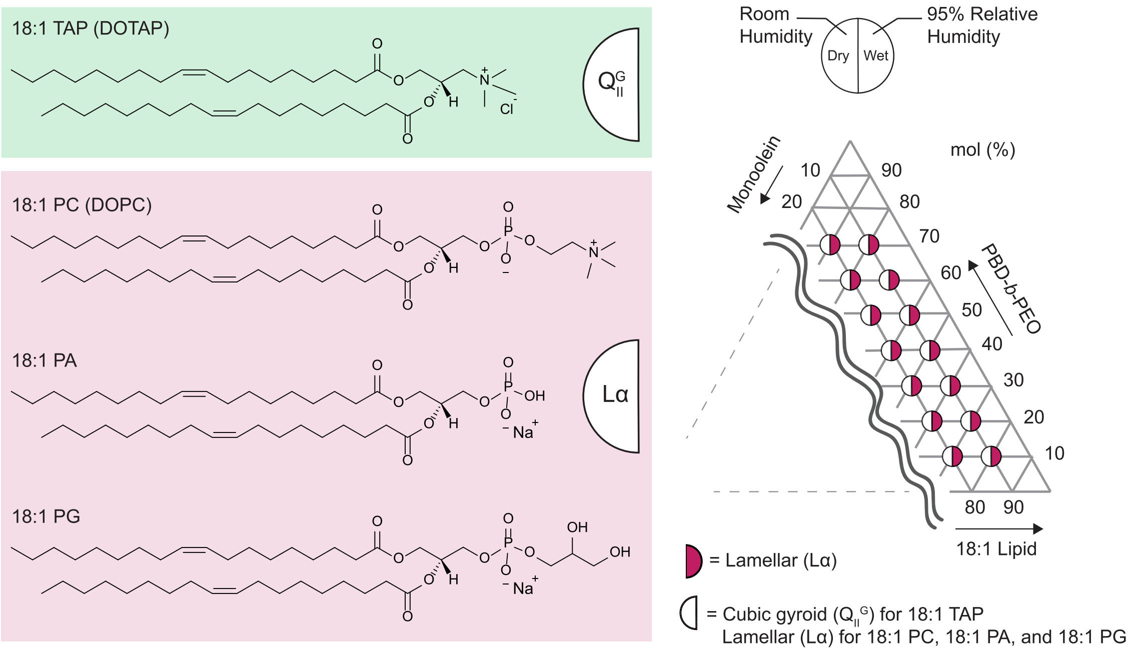

Figure 4. Role of DOTAP in bridging MO and PBD-b-PEO co-assembly. The chemical structures of various 18:1 lipids are shown on the left, while the corresponding phases are shown in a partial ternary phase diagram on the right. The MO/DOTAP/PBD-*b*-PEO systems form the Q_{II}^{G} phase as highlighted in green, whereas MO/18:1 PC or PA or PG/PBD-b-PEO systems form the L_α phase at ambient room humidity as highlighted in red.

the lateral resolution of the ultrasharp AFM tip. This agrees well with the values obtained by SAXS (Figure 2C). To enhance the visualization of the bicontinuous cubic phase AFM topography, rendered Q_{II}^{G} isosurfaces from two different angles are included and overlayed with the AFM high-resolution images (Figure 3G,H). It is noteworthy that the phase image at larger scales precisely overlaps with the features of the topography map (Figure 3A,B). This suggests that the features observed in the topography of MO/DOTAP/PBD-*b*-PEO hybrid films correlate with differences in viscoelasticity. At smaller scales, the phase appears homogeneous (Figure 3F) suggesting domain absence and no phase coexistence.

In order to get further insight into the degree of hybridization of polymers and lipids of a single membrane we utilized a combinatory technique of AFM with Infrared spectroscopy (AFM-IR). We previously employed AFM-IR to investigate the distribution of the anticancer drugs (paclitaxel) in a supported binary lipid−polymer mixture. In this work, paclitaxel IR absorption properties could be distinguished from those of polymers and lipids in the hybrid films.[20,29] AFM-IR enables spectroscopic imaging of local chemical composition from Fourier-transform infrared spectroscopy (FTIR) plus topographic characterization. To evaluate the extent and scale at which a composite material is well-mixed or phase-separated, the individual components must contain chemical bonds that absorb IR in distinct wavelengths. Unfortunately, the three individual components of the MO/DOTAP/PBD-*b*-PEO hybrid material absorb in very similar bands (Supporting Figure 2); therefore, AFM-IR is not completely reliable to elucidate the extent of miscibility or phase separation. However, through AFM-IR experiments, we gained some insights into the composition of the hybrid. First, at larger length scales (Supporting Figure 3A,B), both the IR and phase images exhibit contrast which overlaps with the height features of the topography image of the same sample area. Phase contrast features, which are sensitive to the viscoelastic properties of the components, did not fully overlap with topography or IR maps in the AFM images for some samples. This suggests that there is some degree of material segregation. Several patches appear darker which is indicative of higher local stiffness in the phase map (Supporting Figure 3B). Smaller scale scans on the flattest spots of the topography map (Supporting Figure 3C) display very homogeneous IR maps. It is noteworthy that there is still some contrast in phase that again is not reflected in the topography or the IR maps. In AFM-IR, the depth contrast corresponds to the contrast between equal objects in size and chemical composition located at different depths below the surface.[42] In this case, topography and IR absorption are inversely correlated. Furthermore, the contrast of the objects in the IR maps does not vary, suggesting that these larger aggregates formed on the film absorb less than the flat film itself. This phenomenon is preserved even at comparable small-scale scans ($<1\ \mu$m). The films display domains with IR contrast along with flatter spots that absorb IR homogeneously (Supporting Figure 4). We cannot rule out the possibility that thicker features do not absorb IR effectively as the flat spots due to the higher deflection of the cantilever. Extra AFM-IR maps were recorded at various wavelengths (Supporting Figure 5) with no notable differences.

Since we observed that PBD-*b*-PEO fails to cooperate with MO to form a gyroid cubic phase without the presence of DOTAP, we further explored the role of DOTAP in bridging the interaction between MO and PBD-*b*-PEO. To investigate the role of DOTAP in more detail, we replaced this cationic lipid with unsaturated phospholipids having the same carbon tails (18:1) but different headgroups: 1,2-dioleoyl-*sn*-glycero-3-phosphocholine (DOPC, Zwitterionic), 1,2-dioleoyl-*sn*-glycero-3-phosphate (DOPA, negatively charged), and 1,2-dioleoyl-*sn*-glycero-3-phospho-(1′-rac-glycerol) (DOPG, negatively charged). At fixed MO = 10 or 20 mol %, different formulations of PBD-*b*-PEO and 18:1 lipids were examined for their ability to co-assemble with BCP in hybrid membranes. Remarkably, all three lipids (DOPC, DOPA, DOPG) failed to form bicontinuous cubic phases forming lamellar phases in dry conditions as presented in Figure 4.

It should be noted that in wet conditions (excess water), lipid bicontinuous cubic phases are observed in MO/18:1 lipid binary mixtures. Li et al.[43] showed that the MO/DOPA mixtures form bicontinuous cubic phases (*Pn3m* and *Im3m* space groups) up to 16 mol % of DOPA under excess water conditions. In the case of MO/DOPG mixtures, up to 25 mol % of DOPG can be incorporated into coexisting *Im3m* and *Pn3m* cubic phases.[44]

Only cationic DOTAP, specifically the headgroup TAP, satisfies the required molecular packing for bicontinuous cubic phase formation in dry conditions (ambient room humidity). One of the differences between DOTAP and other 18:1 lipids is that MO/DOTAP exhibits the gyroid cubic phase (Q_{II}^{G}, *Ia3d* space group), whereas MO/DOPA or MO/DOPG shows primitive (*Im3m*) or diamond (*Pn3m*) bicontinuous cubic phases. Gyroid phases require less water to maintain the water channel network compared to primitive or diamond cubic phases at thermodynamic equilibrium.[45] We suggest that PBD-*b*-PEO chains retain the required level of hydration to stabilize the MO/DOTAP gyroid phase but this is insufficient for MO/DOPA or MO/DOPG to sustain the primitive or diamond phases. In addition, positively charged DOTAP lipids are expected to facilitate electrostatic interactions among ethylene oxides in PBD-*b*-PEO and glycerol in MO.

To validate the proposed underlying mechanisms of the formation of stable gyroid cubic phases at ambient room humidity, we performed coarse-grained simulations using the Martini force field.[46,47] In these simulations, we used a cylindrical cut-out capped by an elastically bound wall representing the water nanochannels of the bicontinuous cubic phase (Figure 5A). The elastically bound wall was composed of C1-type beads to prevent particles from crossing as shown in gray in Figure 5A. Lipid MO and DOTAP headgroups, PEO chains, water, and chlorine ions (counterions of DOTAP lipid headgroups) were explicitly represented. Simulation methods and parameters are described in detail in the Experimental Section.

We evaluated different levels of hydration (*i.e.*, number of water molecules per lipid molecule) inside the small channel and found that the channel with two or four PEO chains exhibit larger volumes at all levels of hydration (Figure 5B). This is consistent with our previous findings that lipids covalently linked to poly(ethylene glycol) (PEG) can swell an MO bicontinuous cubic phase.[48,49] We attribute this to three factors: (1) the PEO chains provide steric hindrance and take up volume inside of the channel, (2) the lipid-bilayer is more flexible and consequently stretches further when it contains PBD-*b*-PEO, and (3) the PEO chains retain some water and provide sites for the Cl^- ions, as the channel is dehydrated (further discussed in Figure 5C). Using m tessellation, we determined the nearest neighbors of different species in the equilibrated water channel (Figure 5C).[50,51] Fairly independent of the level of hydration, the PEO chains are neighbored by water molecules, proportional to the amount of PEO chains, *e.g.*, the PEO chains help bind some water in the channel. As the channel is dehydrated, the Cl ions have less and less water neighbors, and instead condense more and more onto the positively charged DOTAP headgroups and PEO chains. As the number of PEO chains is increased, the Cl^- ions show more condensation onto DOTAP and PEO. Due to the opposite charges of DOTAP and Cl, this provides a small energetic benefit as the Cl^- ions lose their hydrated environment as hydration levels decrease. We also show that the contribution of flexibility is more important for highly swollen channels, whereas the steric volume contributions from the presence of PEO in the channel are dominating for more dehydrated channels (Supporting Figure 6).

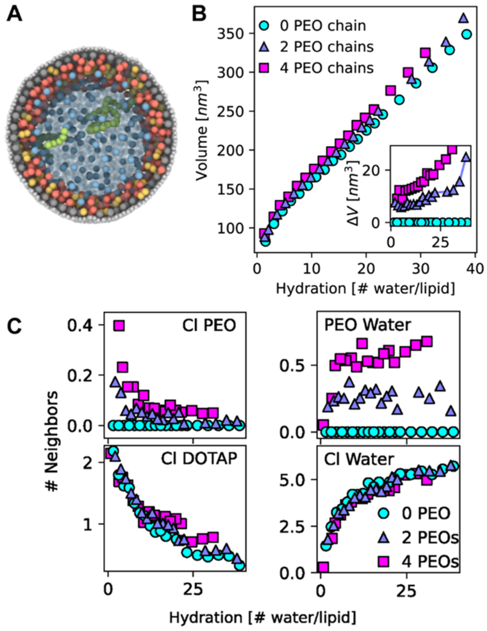

Figure 5. Coarse-grained simulations on water channels of MO/DOTAP/PBD-*b*-PEO cubic phases. (A) Snapshot of a typical configuration with 2 PEO chains at a hydration level of 19.2 water molecules per lipid. MO headgroups are in yellow, DOTAP headgroups are in red, PEO is shown in green, Cl^- ions are in blue, hydrocarbon chains are in gray, and wall beads are shown in light gray. The water beads are rendered transparent and bead sizes are slightly reduced for visual clarity. (B) Volume of channel as a function of hydration (# water molecules per lipid molecule) for zero, two, or four PEO chains in the channel. The inset shows the volume difference ΔV to the channel without any PEO added. (C) Number of neighbors of different types (e.g., Cl-PEO, PEO-water, Cl-DOTAP, and Cl-water) as a function of hydration for different number of PEO chains, as indicated.

Altogether, GISAXS, GIWAXS, AFM, and AFM-IR data indicate that, at the sub-nanoscale, lipids and BCPs mix molecularly into a hybrid bilayer form. Coarse-grained simulations are consistent with the proposed mechanisms for the stabilization of a bicontinuous cubic phase at low relative humidity where the molecular interactions among PEO chains, lipid headgroups, and counterions prevent the collapse of water channels. Zooming out at larger scales (>1 μm) these hybrid bilayers are separated into two distinct mesoscale domains: one comprises lipid-rich (but containing polymers) hybrid bilayers folded into a bicontinuous cubic structure and another is composed of polymer-rich (but containing lipids) hybrid bilayers that stack into a lamellar phase. A proposed hybrid film structure (MO/DOTAP/PBD-*b*-PEO when MO = 20 mol %) is illustrated in Figure 6 summarizing our findings.

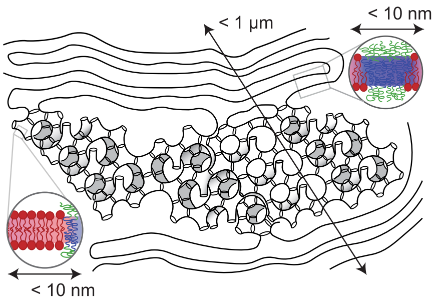

Figure 6. Schematic illustration of the structure of hybrid MO/DOTAP/PBD-*b*-PEO supported thin films at ambient room humidity. The gyroid cubic phase (lipid-rich) forms micron-sized domains surrounded by flat polymer-rich lamellar layers. At the nanoscale, lipids and BCPs are molecularly mixed in a hybrid bilayer.

■ CONCLUSIONS

In conclusion, mixing lipids (MO, DOTAP) and block copolymers (PBD-*b*-PEO) to form solid-supported thin films resulted in the formation of various nanostructures, most notably bicontinuous cubic phases in dry air. The intricate interplay between each component enabled the stabilization of inverse bicontinuous gyroid cubic phases in an open environment at ambient room humidity, unattainable in single-component lipid or BCP thin films. Through AFM experiments we could visualize the gyroid cubic phase in air and resolve the spacing between water channels (a = 9 nm), corroborated with the lattice parameter of the cubic phase obtained by GISAXS. Using coarse-grained simulations, we demonstrated that the presence of PEO chains facilitates water retention within the channel networks during the dehydration process. We also showed that the positively charged DOTAP headgroups and PEO chains provide sites for Cl^- ions as hydration levels decrease wherein the opposite charges of DOTAP and Cl provide an energetic benefit upon Cl^- ions losing their hydrated environment. Our findings of a dry bicontinuous cubic phase rich in lipids by hybridization with block copolymers have the potential to unlock future applications of lipid−polymer hybrid systems ranging from separation membranes to drug delivery while providing new insight into the fundamental co-assembly behavior of amphiphilic lipids and block copolymer into supramolecular hybrid constructs.

■ EXPERIMENTAL SECTION

Materials. Glyceryl monooleate (MO) was purchased from NU-CHEK PREP, Inc. (Elysian, MN). 1,2-dioleoyl-3-trimethylammoniumpropane (DOTAP), 1,2-dioleoyl-*sn*-glycero-3-phosphocholine (DOPC), 1,2-dioleoyl-*sn*-glycero-3-phosphate (DOPA), and 1,2-dioleoyl-*sn*-glycero-3-phospho-(1′-rac-glycerol) (DOPG) were purchased from Avanti Polar Lipids (Alabaster, AL). All lipids were used without further purification. Amphiphilic diblock copolymer, poly(butadiene-*b*-ethylene oxide) (PBD-*b*-PEO), was purchased from Polymer Source, Inc. (Quebec, Canada). The catalog number is P19015-BdEO. Its average molecular weight (M_n) was reported to be 4000 with PBD block (rich in 1,4 microstructure) 2500 and PEO block 1500, respectively. The reported polydispersity was 1.06.

Atomic Force Microscopy (AFM). Thin films composed of lipids, block copolymers, and their hybrids were prepared by spin-coating methods for atomic force microscopy (AFM) analyses. Both lipids and block copolymers were dissolved in chloroform (~25 mg/mL). A stock solution was made with a desired composition by mixing each component. The stock solution of 80 μL was spin-coated onto a silicon wafer (1×1 cm^2) at 3000 rpm for 30 s. To fully remove the solvent, the film samples were kept in a vacuum desiccator overnight. This solvent evaporation is for a self-assembly of lipids/block copolymer hybrids by their intrinsic nature, toward cubic phase formation. The silicon wafer substrates are boron-doped P-type Si wafers with ⟨100⟩ orientation and were purchased from University Wafer, Inc. (South Boston; MA). For AFM scanning, we employed high-resolution silicon tapping mode AFM tips (SHR300, Budget Sensors) with a typical spike tip radius of 1 nm. For AFM-IR experiments, we used silicon noncontact mode with Pt/Ir-coating on tip and detector sides (ARROW-NCPt-10, NanoWorld).

Grazing Incidence Small-Angle X-ray Scattering (GISAXS). Hybrid films composed of MO, DOTAP, PBD-*b*-PEO were prepared by drop-casting methods. Stock solutions were prepared in chloroform/ethanol mixtures (4:1 volume ratio). The stock solution was dropped onto the substrate followed by a solvent evaporation under a fume hood. The experiments were carried out at in-house X-ray setup (custom-built with the help of Forvis Technologies, CA) and at 12-ID-B beamline, Advanced Photon Source (APS), Argonne National Laboratory. A custom-built (with Forvis Technologies, Santa Barbara) equipment composed of a Xenocs GeniX3D Cu Kα ultralow divergence X-ray source (8 keV) was used, with a divergence of 1.3 mrad. The humidity and temperature control chambers were built by Forvis Technologies. At the 12-ID-B beamline APS, a 14 keV X-ray beam was focused on a 50×10 μm^2 ($H \times V$) area at an incident angle of 0.05−0.2°. Pilatus2M (Dectris) and PerkinElmer XRPad 4343F detectors were used for GISAXS and GIWAXS measurements, respectively. The sample-to-detector distance was calibrated using a silver behenate powder standard. The specular beam intensity was attenuated along the z axis with a strip beam stop. The sample-to-detector distance for GISAXS was either 2 or 3.6 m, and that for GIWAXS was about 0.15 m. Multiple measurements (N = 5) were carried out on samples inside a humidity chamber (relative humidity >95%), varying the incidence angle to determine the most appropriate operating angle.

Simulation Model and Methods. We performed coarse-grained simulations using the Martini v2.2 lipid force field.[46,47] This model has been used previously for PEO,[52] DOTAP,[53] and MO.[54] Because the entire unit cell of the inverted bicontinuous phase contains too many molecules to be simulated in full, we focus on a small section of the inside of one of the water channels, which we cap by an elastically bound wall (harmonic bonds with r_0 = 0.2 nm, k = 500−2000 kJ mol^{-1} nm^{-2} depending on the number of PEO chains) made out of C1-type beads, which were scaled to σ = 0.32 nm and otherwise interact like conventional C1 beads, to prevent particles from crossing representing the lipid tails that would normally form the bilayer. The wall elasticity was varied by tuning the harmonic potential spring constant from 500 to 2000 kJ/(mol × nm^2) to account for the elasticity decrease when adding PBD-PEO to a lipid membrane.[55] The lipid headgroups, PEO chains, water, and chlorine ions are represented explicitly. Note that the Martini force field only represents screened charged interactions and does not explicitly account for hydrogen bonding, as the hydrogens are incorporated in the coarse-grained bead and not represented explicitly. The PEO end-group of each chain was strongly attracted to the walls (ϵ = 6.0 kJ/mol), to ensure that they stayed bound to the lipid layer. Each lipid was explicitly represented up to their first C1 carbon tail bead, creating a stable liquid-like monolayer coating on the inside of the wall, representing the top interface of the bilayer. This also automatically leads to the correct area per lipid headgroup (0.31 nm^2 for MO[56] and 0.71 nm^2 for DOTAP[57] measured experimentally), where DOTAP is taking up about twice as much area as MO. We initialized the channel with h = 5 nm and R = 5 nm and used 172 DOTAP and 85 MO beads, which would add up to approx. 148 nm^2 of lipid area. This leads to about 10 nm^2 flexibility in surface, which accounts for PEO chains and allows the membrane layer to relax from its initial perfectly stretched cylindrical surface. With this setup, we then varied the amount of PEO (each chain has a length of 35 beads, corresponding to the experimental chain length). The overall simulation box was filled with water at a constant density of 1000 kg/m^3 to ensure pressure equilibrium. We also changed the degree of hydration inside of the channel by removing or adding beads from outside the channel to the inside, while keeping the total density in the simulation box of total volume 5 nm × 15 nm × 15 nm constant. The water contained 10% antifreeze beads[46,58] to prevent artificial crystallization at the wall surface. Each system was equilibrated for 20 ns in the NVT ensemble with a timestep of 0.02 ps at 298.15 K. After equilibration, the size of the channel was measured based on the positions of the first hydrocarbon tail beads in each lipid. The level of hydration was calculated by determining the number of water molecules inside the channel, normalized by the number of lipids. We assume a cylindrical shape for the channel, which is accurate (as shown in Supporting Figure 6), up until low levels of hydration, where the channel starts to collapse on itself.

■ ASSOCIATED CONTENT

Supporting Information

The Supporting Information is available free of charge at https://pubs.acs.org/doi/10.1021/acs.macromol.3c00239.

> GIWAXS, FTIR, and AFM-IR spectra of a supported lipid−polymer hybrid film, and coarse-grained simulation data on the difference in volumes ΔV to the water channel as a function of hydration (PDF)

■ AUTHOR INFORMATION

Corresponding Authors

Antonia Statt − *Department of Materials Science and Engineering, University of Illinois Urbana-Champaign, Urbana, Illinois 61801, United States;* orcid.org/0000-0002-6120-5072; Email: statt@illinois.edu

Cecilia Leal − *Department of Materials Science and Engineering, University of Illinois Urbana-Champaign, Urbana, Illinois 61801, United States;* orcid.org/0000-0001-5972-508X; Email: cecilial@illinois.edu

Authors

Minjee Kang − *Division of Oral and Systemic Health Sciences, School of Dentistry, University of California, Los Angeles, Los Angeles, California 90095, United States;* orcid.org/0000-0002-0581-4105

Yoo Kyung Go − *Department of Materials Science and Engineering, University of Illinois Urbana-Champaign, Urbana, Illinois 61801, United States;* orcid.org/0000-0002-6779-0225

Marilyn Porras-Gomez − *Department of Materials Science and Engineering, University of Illinois Urbana-Champaign, Urbana, Illinois 61801, United States;* orcid.org/0000-0002-1601-1308

Tzortzis Koulaxizis − *Department of Chemical and Biomolecular Engineering, University of Illinois at Urbana-Champaign, Urbana, Illinois 61801, United States*

Dylan Steer − *Department of Materials Science and Engineering, University of Illinois Urbana-Champaign, Urbana, Illinois 61801, United States*

Complete contact information is available at: https://pubs.acs.org/10.1021/acs.macromol.3c00239

Author Contributions

The manuscript was written through contributions of all authors. All authors have given approval to the final version of the manuscript.

Notes

The authors declare no competing financial interest.

■ ACKNOWLEDGMENTS

This work was supported by the National Science Foundation under Award No. CBET 2219305 and ACS-PRF 65334-DNI7 (computer simulations). Synchrotron X-ray experiments were carried out at beamline 12-ID-B at the Advanced Photon Source (APS), Argonne National Laboratory. The use of APS was supported by the US Department of Energy (DOE), Office of Science, Office of Basic Energy Sciences, under Contract No. DE-AC02-06CH11357. This research was carried out in part in the Materials Research Laboratory Central Research Facilities, University of Illinois Urbana−Champaign.

■ REFERENCES

(1) Go, Y. K.; Leal, C. Polymer−Lipid Hybrid Materials. *Chem. Rev.* **2021**, *121*, 13996−14030.

(2) Go, Y. K.; Shin, J.; Chen, G.; Leal, C. Reorientation of Crystalline Block Copolymer Membranes by Phospholipid Hybridization. *Chem. Mater.* **2022**, *34*, 8577−8592.

(3) Le Meins, J.-F.; Schatz, C.; Lecommandoux, S.; Sandre, O. Hybrid Polymer/Lipid Vesicles: State of the Art and Future Perspectives. *Mater. Today* **2013**, *16*, 397−402.

(4) Lim, S.; de Hoog, H.-P.; Parikh, A.; Nallani, M.; Liedberg, B. Hybrid, Nanoscale Phospholipid/Block Copolymer Vesicles. *Polymers* **2013**, *5*, 1102−1114.

(5) Schulz, M.; Binder, W. H. Mixed Hybrid Lipid/Polymer Vesicles as a Novel Membrane Platform. *Macromol. Rapid Commun.* **2015**, *36*, 2031−2041.

(6) Beales, P. A.; Khan, S.; Muench, S. P.; Jeuken, L. J. C. Durable Vesicles for Reconstitution of Membrane Proteins in Biotechnology. *Biochem. Soc. Trans.* **2017**, *45*, 15−26.

(7) Dao, T. P. T.; Ferji, K.; Fernandes, F.; Prieto, M.; Lecommandoux, S.; Ibarboure, E.; Sandre, O.; Meins, J.-F. L. Giant Hybrid Polymer/Lipid Vesicles. In *The Giant Vesicle Book*; Dimova, R.; Marques, C. M., Eds.; CRC Press, Taylor & Francis Group: CRC Press: Boca Raton, FL, 2020; Vol. *2019*, pp 551−568.

(8) Krywko-Cendrowska, A.; Di Leone, S.; Bina, M.; Yorulmaz-Avsar, S.; Palivan, C. G.; Meier, W. Recent Advances in Hybrid Biomimetic Polymer-Based Films: From Assembly to Applications. *Polymers* **2020**, *12*, No. 1003.

(9) Khan, S.; McCabe, J.; Hill, K.; Beales, P. A. Biodegradable Hybrid Block Copolymer − Lipid Vesicles as Potential Drug Delivery Systems. *J. Colloid Interface Sci.* **2020**, *562*, 418−428.

(10) De Leo, V.; Milano, F.; Agostiano, A.; Catucci, L. Recent Advancements in Polymer/Liposome Assembly for Drug Delivery: From Surface Modifications to Hybrid Vesicles. *Polymers* **2021**, *13*, No. 1027.

(11) Marušič, N.; Otrin, L.; Zhao, Z.; Lira, R. B.; Kyrilis, F. L.; Hamdi, F.; Kastritis, P. L.; Vidaković-Koch, T.; Ivanov, I.; Sundmacher, K.; et al. Constructing Artificial Respiratory Chain in Polymer Compartments: Insights into the Interplay between Bo 3 Oxidase and the Membrane. *Proc. Natl. Acad. Sci. U.S.A.* **2020**, *117*, 15006−15017.

(12) Bates, C. M.; Bates, F. S. 50th *Anniversary Perspective*: Block Polymers—Pure Potential. *Macromolecules* **2017**, *50*, 3−22.

(13) Chen, D.; Santore, M. M. Hybrid Copolymer−Phospholipid Vesicles: Phase Separation Resembling Mixed Phospholipid Lamellae, but with Mechanical Stability and Control. *Soft Matter* **2015**, *11*, 2617−2626.

(14) Kang, J. Y.; Choi, I.; Seo, M.; Lee, J. Y.; Hong, S.; Gong, G.; Shin, S. S.; Lee, Y.; Kim, J. W. Enhancing Membrane Modulus of Giant Unilamellar Lipid Vesicles by Lateral Co-Assembly of Amphiphilic Triblock Copolymers. *J. Colloid Interface Sci.* **2020**, *561*, 318−326.

(15) Fauquignon, M.; Ibarboure, E.; Le Meins, J.-F. Membrane Reinforcement in Giant Hybrid Polymer Lipid Vesicles Achieved by Controlling the Polymer Architecture. *Soft Matter* **2021**, *17*, 83−89.

(16) Olubummo, A.; Schulz, M.; Lechner, B.-D.; Scholtysek, P.; Bacia, K.; Blume, A.; Kressler, J.; Binder, W. H. Controlling the Localization of Polymer-Functionalized Nanoparticles in Mixed Lipid/Polymer Membranes. *ACS Nano* **2012**, *6*, 8713−8727.

(17) Schulz, M.; Olubummo, A.; Bacia, K.; Binder, W. H. Lateral Surface Engineering of Hybrid Lipid−BCP Vesicles and Selective Nanoparticle Embedding. *Soft Matter* **2014**, *10*, 831−839.

(18) Kowal, J.; Wu, D.; Mikhalevich, V.; Palivan, C. G.; Meier, W. Hybrid Polymer−Lipid Films as Platforms for Directed Membrane Protein Insertion. *Langmuir* **2015**, *31*, 4868−4877.

(19) Fauquignon, M.; Courtecuisse, E.; Josselin, R.; Mutschler, A.; Brûlet, A.; Schmutz, M.; Le Meins, J.-F. Large Hybrid Polymer/Lipid Unilamellar Vesicle (LHUV) at the Nanoscale: An Insight into the Lipid Distribution in the Membrane and Permeability Control. *J. Colloid Interface Sci.* **2021**, *604*, 575−583.

(20) Tuteja, M.; Kang, M.; Leal, C.; Centrone, A. Nanoscale Partitioning of Paclitaxel in Hybrid Lipid−Polymer Membranes. *Analyst* **2018**, *143*, 3808−3813.

(21) Kang, M.; Lee, B.; Leal, C. Three-Dimensional Microphase Separation and Synergistic Permeability in Stacked Lipid−Polymer Hybrid Membranes. *Chem. Mater.* **2017**, *29*, 9120−9132.

(22) Paxton, W. F.; McAninch, P. T.; Achyuthan, K. E.; Shin, S. H. R.; Monteith, H. L. Monitoring and Modulating Ion Traffic in Hybrid Lipid/Polymer Vesicles. *Colloids Surf., B* **2017**, *159*, 268−276.

(23) Go, Y. K.; Kambar, N.; Leal, C. Hybrid Unilamellar Vesicles of Phospholipids and Block Copolymers with Crystalline Domains. *Polymers* **2020**, *12*, No. 1232.

(24) Nam, J.; Beales, P. A.; Vanderlick, T. K. Giant Phospholipid/Block Copolymer Hybrid Vesicles: Mixing Behavior and Domain Formation. *Langmuir* **2011**, *27*, 1−6.

(25) Nam, J.; Vanderlick, T. K.; Beales, P. A. Formation and Dissolution of Phospholipid Domains with Varying Textures in Hybrid Lipo-Polymersomes. *Soft Matter* **2012**, *8*, No. 7982.

(26) Gettel, D. L.; Sanborn, J.; Patel, M. A.; de Hoog, H.-P.; Liedberg, B.; Nallani, M.; Parikh, A. N. Mixing, Diffusion, and Percolation in Binary Supported Membranes Containing Mixtures of Lipids and Amphiphilic Block Copolymers. *J. Am. Chem. Soc.* **2014**, *136*, 10186−10189.

(27) Di Leone, S.; Kyropoulou, M.; Köchlin, J.; Wehr, R.; Meier, W. P.; Palivan, C. G. Tailoring a Solvent-Assisted Method for Solid-Supported Hybrid Lipid−Polymer Membranes. *Langmuir* **2022**, *38*, 6561−6570.

(28) Kambar, N.; Leal, C. Microfluidic Synthesis of Multilayered Lipid−Polymer Hybrid Nanoparticles for the Formulation of Low Solubility Drugs. *Soft Matter* **2023**, *19*, 1596−1605.

(29) Kang, M.; Tuteja, M.; Centrone, A.; Topgaard, D.; Leal, C. Nanostructured Lipid-Based Films for Substrate-Mediated Applications in Biotechnology. *Adv. Funct. Mater.* **2018**, *28*, No. 1704356.

(30) Bender, J.; Ericson, M. B.; Merclin, N.; Iani, V.; Ros?n, A.; Engström, S.; Moan, J. Lipid Cubic Phases for Improved Topical Drug Delivery in Photodynamic Therapy. *J. Controlled Release* **2005**, *106*, 350−360.

(31) Landau, E. M.; Rosenbusch, J. P. Lipidic Cubic Phases: A Novel Concept for the Crystallization of Membrane Proteins. *Proc. Natl. Acad. Sci. U.S.A.* **1996**, *93*, 14532−14535.

(32) Vallooran, J. J.; Handschin, S.; Pillai, S. M.; Vetter, B. N.; Rusch, S.; Beck, H.-P.; Mezzenga, R. Lipidic Cubic Phases as a Versatile Platform for the Rapid Detection of Biomarkers, Viruses, Bacteria, and Parasites. *Adv. Funct. Mater.* **2016**, *26*, 181−190.

(33) Feng, X.; Imran, Q.; Zhang, Y.; Sixdenier, L.; Lu, X.; Kaufman, G.; Gabinet, U.; Kawabata, K.; Elimelech, M.; Osuji, C. O. Precise Nanofiltration in a Fouling-Resistant Self-Assembled Membrane with Water-Continuous Transport Pathways. *Sci. Adv.* **2019**, *5*, No. eaav9308.

(34) Rittman, M.; Amenitsch, H.; Rappolt, M.; Sartori, B.; O'Driscoll, B. M. D.; Squires, A. M. Control and Analysis of Oriented Thin Films of Lipid Inverse Bicontinuous Cubic Phases Using Grazing Incidence Small-Angle X-Ray Scattering. *Langmuir* **2013**, *29*, 9874−9880.

(35) Takeuchi, R.; Ichikawa, T. Improvement of Lipidic Bicontinuous Cubic Phases by the Addition of a Zwitterion with Strong Hydration Ability and Kosmotropicity. *New J. Chem.* **2019**, *43*, 3084−3090.

(36) Richardson, S. J.; Staniec, P. A.; Newby, G. E.; Rawle, J. L.; Slaughter, A. R.; Terrill, N. J.; Elliott, J. M.; Squires, A. M. Glycerol Prevents Dehydration in Lipid Cubic Phases. *Chem. Commun.* **2015**, *51*, 11386−11389.

(37) Leal, C.; Bouxsein, N. F.; Ewert, K. K.; Safinya, C. R. Highly Efficient Gene Silencing Activity of SiRNA Embedded in a Nanostructured Gyroid Cubic Lipid Matrix. *J. Am. Chem. Soc.* **2010**, *132*, 16841−16847.

(38) Kang, M.; Leal, C. Soft Nanostructured Films for Actuated Surface-Based SiRNA Delivery. *Adv. Funct. Mater.* **2016**, *26*, 5610−5620.

(39) He, F.; Tong, Y. W. A Mechanistic Study on Amphiphilic Block Co-Polymer Poly(Butadiene-b-(Ethylene Oxide)) Vesicles Reveals the Water Permeation Mechanism through a Polymeric Bilayer. *RSC Adv.* **2014**, *4*, 15304−15313.

(40) Hu, J.; Yamahara, H.; Liao, Z.; Yano, Y.; Tabata, H. Characterization of Hydrogen Bond Network of Waters around Polyethylene Glycol by Broadband Dielectric Spectroscopy. *Appl. Phys. Lett.* **2022**, *120*, No. 023702.

(41) Kulkarni, C. V.; Wachter, W.; Iglesias-Salto, G.; Engelskirchen, S.; Ahualli, S. Monoolein: A Magic Lipid? *Phys. Chem. Chem. Phys.* **2011**, *13*, 3004−3021.

(42) Krutokhvostov, R.; Govyadinov, A. A.; Stiegler, J. M.; Huth, F.; Chuvilin, A.; Carney, P. S.; Hillenbrand, R. Enhanced Resolution in Subsurface Near-Field Optical Microscopy. *Opt. Express* **2012**, *20*, No. 593.

(43) Li, S. J.; Yamashita, Y.; Yamazaki, M. Effect of Electrostatic Interactions on Phase Stability of Cubic Phases of Membranes of Monoolein/Dioleoylphosphatidic Acid Mixtures. *Biophys. J.* **2001**, *81*, 983−993.

(44) Brasnett, C.; Longstaff, G.; Compton, L.; Seddon, A. Effects of Cations on the Behaviour of Lipid Cubic Phases. *Sci. Rep.* **2017**, *7*, No. 8229.

(45) Qiu, H.; Caffrey, M. The Phase Diagram of the Monoolein/Water System: Metastability and Equilibrium Aspects. *Biomaterials* **2000**, *21*, 223−234.

(46) Marrink, S. J.; Risselada, H. J.; Yefimov, S.; Tieleman, D. P.; de Vries, A. H. The MARTINI Force Field: Coarse Grained Model for Biomolecular Simulations. *J. Phys. Chem. B* **2007**, *111*, 7812−7824.

(47) Marrink, S. J.; De Vries, A. H.; Mark, A. E. Coarse Grained Model for Semiquantitative Lipid Simulations. *J. Phys. Chem. B* **2004**, *108*, 750−760.

(48) Kim, H.; Song, Z.; Leal, C. Super-Swelled Lyotropic Single Crystals. *Proc. Natl. Acad. Sci. U.S.A.* **2017**, *114*, 10834−10839.

(49) Leung, S. S. W.; Leal, C. The Stabilization of Primitive Bicontinuous Cubic Phases with Tunable Swelling over a Wide Composition Range. *Soft Matter* **2019**, *15*, 1269−1277.

(50) Ramasubramani, V.; Dice, B. D.; Harper, E. S.; Spellings, M. P.; Anderson, J. A.; Glotzer, S. C. Freud: A Software Suite for High Throughput Analysis of Particle Simulation Data. *Comput. Phys. Commun.* **2020**, *254*, No. 107275.

(51) Barber, C. B.; Dobkin, D. P.; Huhdanpaa, H. The Quickhull Algorithm for Convex Hulls. *ACM Trans. Math. Software* **1996**, *22*, 469−483.

(52) Grunewald, F.; Rossi, G.; De Vries, A. H.; Marrink, S. J.; Monticelli, L. Transferable MARTINI Model of Poly(Ethylene Oxide). *J. Phys. Chem. B* **2018**, *122*, 7436−7449.

(53) Sun, L.; Mao, J.; Zhao, Y.; Quan, C.; Zhong, M.; Fan, S. Coarse-Grained Molecular Dynamics Simulation of Interactions between Cyclic Lipopeptide Bacillomycin D and Cell Membranes. *Mol. Simul.* **2018**, *44*, 364−376.

(54) Green, N. L.; Euston, S. R.; Rousseau, D. Interfacial Ordering of Tristearin Induced by Glycerol Monooleate and PGPR: A Coarse-Grained Molecular Dynamics Study. *Colloids Surf., B* **2019**, *179*, 107−113.

(55) Steinkühler, J.; Jacobs, M. L.; Boyd, M. A.; Villaseñor, C. G.; Loverde, S. M.; Kamat, N. P. PEO- *b* -PBD Diblock Copolymers Induce Packing Defects in Lipid/Hybrid Membranes and Improve Insertion Rates of Natively Folded Peptides. *Biomacromolecules* **2022**, *23*, 4756−4765.

(56) Reese, C. W.; Strango, Z. I.; Dell, Z. R.; Tristram-Nagle, S.; Harper, P. E. Structural Insights into the Cubic−Hexagonal Phase Transition Kinetics of Monoolein Modulated by Sucrose Solutions. *Phys. Chem. Chem. Phys.* **2015**, *17*, 9194−9204.

(57) Gurtovenko, A. A.; Patra, M.; Karttunen, M.; Vattulainen, I. Cationic DMPC/DMTAP Lipid Bilayers: Molecular Dynamics Study. *Biophys. J.* **2004**, *86*, 3461−3472.

(58) Potter, T. D.; Barrett, E. L.; Miller, M. A. Automated Coarse-Grained Mapping Algorithm for the Martini Force Field and Benchmarks for Membrane−Water Partitioning. *J. Chem. Theory Comput.* **2021**, *17*, 5777−5791.

https://doi.org/10.1021/acs.macromol.3c00239
Macromolecules 2023, 56, 5774−5783